A Mass Spectrometric Approach to the Study of DNA-Binding Proteins: Interaction of Human TRF2 with Telomeric DNA[†]

Justin B. Sperry,[‡] Xiangguo Shi,[§] Don L. Rempel,[‡] Yoshifumi Nishimura,[∥] Satoko Akashi,[∥] and Michael L. Gross*[,‡]

Department of Chemistry, Washington University, St. Louis, Missouri 63130, Rowland Institute at Harvard, Cambridge, Massachusetts 02142, and Yokohama City University, Tsurumi-ku, Yokohama 230-0045, Japan

Received October 10, 2007; Revised Manuscript Received November 19, 2007

ABSTRACT: Human telomeric repeat binding factor 2 (hTRF2) is a protein that plays an important role in capping human telomeres to protect them from DNA damage repair systems. The ineffectiveness of hTRF2 may be linked to aging and cancer. We report the use of PLIMSTEX (protein−ligand interactions by mass spectrometry, titration, and H/D exchange) and selective acetylation of lysine residues to study the interaction of the DNA-binding domain and double-stranded telomeric DNA (repeats of TTAGGG). By increasing the resolution of PLIMSTEX to the peptide level, we localized the changes in deuterium uptake of hTRF2 as a function of varying amounts of a model oligodeoxynucleotide. From these experiments, we determined the affinity constant for binding to DNA, which is within a factor of 3 of the previously reported value. Amide H/D exchange revealed portions of the protein that have contacts with the phosphate backbone of DNA, whereas acetylation disclosed the decrease in solvent accessibility of regions containing Lys 447 and 488, which must be involved in interactions with the DNA major and minor grooves. These complementary approaches of amide H/D exchange and selective side chain modification can be employed effectively to pinpoint and quantify protein−ligand, in particular protein−DNA, interactions.

Portions of human telomeres are protein−DNA complexes that protect and replicate eukaryotic linear chromosomes. The telomeres contain multi-kilobase tandem arrays of TTAGGG repeats that bind human telomeric repeat binding factors 1 and 2. The cell utilizes the protein−DNA complex to distinguish a natural chromosome end from one that is broken from DNA damage (*1*−*3*). The primary function of hTRF1[1] is to regulate telomere access by telomerase, a DNA polymerase that is responsible for the elongation of telomeres (*4*, *5*). Although hTRF2 is also responsible for regulating telomere length (*5*), it also has been implicated in forming a t-loop, considered to be a type of telomeric higher-order structure (*6*, *7*). Furthermore, the altered function of this protein may be linked to premature aging and some forms of cancer (*8*).

For proteins like hTRF2, the study of domains is often the productive approach. X-ray and NMR structures of full-length hTRF2 are not known, in this case, because of a characteristic unstructured linker between the DNA-binding domain and the TRF homology sequence. The protein has four distinct regions: the basic N-terminal domain, the TRF homology sequence (residues 45−245), the unstructured linker (residues 246−445), and the DNA-binding domain (residues 446−500) (*2*). In fact, the structure of the TRF homology sequence, also characterized as a dimerization domain, was determined by X-ray diffraction (*9*), and the structure of the DNA-binding domain containing a portion of the unstructured linker was determined by NMR and X-ray crystallography (*10*−*14*). Three helices make up the DNA-binding domain. The major groove of telomeric DNA is bound by the third helix, which contains a highly positively charged region comprised of two lysines and three arginines. A minor groove interaction involves a small portion of the unstructured linker (*12*, *15*). Amide contacts with the phosphate backbone are also present in helices 1 and 2 (*15*).

Mass spectrometric techniques that reveal changes in the solvent accessibility of proteins that bind to DNA and determine affinities would be particularly valuable because of the speed and sensitivity of MS. Such an approach to tertiary structure is not hindered by unstructured regions, thus making the approach more amenable to proteins that are difficult to crystallize. One evolving approach combines amide hydrogen exchange and mass spectrometry (*16*−*20*). PLIMSTEX (protein−ligand interactions by mass spectrom-

[†] These studies were supported by the National Institutes of Health and National Center for Research Resources (Grant P41RR00954 to M.L.G.), by the Project of Protein 3000; Transcription and Translation (to Y.N.), and by Grants-in-Aid for Scientific Research (MEXT) (to S.A. and Y.N.).

* To whom correspondence should be addressed: Department of Chemistry, Washington University, Campus Box 1134, St. Louis, MO 63130. Telephone: (314) 935-4814. Fax: (314) 935-7484. E-mail: mgross@wustl.edu.

[‡] Washington University.

[§] Rowland Institute at Harvard.

[∥] Yokohama City University.

[1] Abbreviations: H/D, hydrogen−deuterium; hTRF1, human telomeric repeat binding factor 1; hTRF2, human telomeric repeat binding factor 2; ODN, oligodeoxynucleotide; PLIMSTEX, protein−ligand interactions by mass spectrometry, titration, and H−D exchange; ESI-MS, electrospray ionization mass spectrometry; NMR, nuclear magnetic resonance; SPR, surface plasmon resonance; IPTG, isopropyl 1-thio-*β*-D-galactopyranoside; HEPES, *N*-(2-hydoxyethyl)piperazine-*N*′-2-ethanesulfonic acid; EDTA, ethylenediaminetetraacetic acid; KCl, potassium chloride; NaCl, sodium chloride; HCl, hydrochloric acid; Q-TOF, quadrupole time-of-flight.

10.1021/bi702037p CCC: $40.75 © 2008 American Chemical Society
Published on Web 01/16/2008

etry, titration, and H/D exchange) is a refinement of that approach, affording binding affinities of proteins and their ligands in solution (not in the gas phase), their binding stoichiometry, and a measure of the conformational changes that occur in the protein upon ligand binding. Amide H/D exchange rates can be monitored by determining the mass change (ΔD) upon equilibrium titration of the protein with ligand. Usually, ΔD decreases because ligand binding is accompanied by protection from solvent and/or an increase in the extent of hydrogen bonding (*21*−*23*).

Once a global view of protein protection is obtained by H/D exchange, the spatial resolution of the deuterium uptake can be increased by proteolyzing the labeled protein with pepsin after the exchange is quenched and analyzing the peptides by MS (*24*, *25*). Mass analysis of the peptic peptides should provide high-resolution deuterium uptake information. If the H/D exchange rates of amide sites in the protein do not change upon ligand binding, they will show little change in ΔD, whereas for those sites where hydrogen bonding does change, the H/D exchange rate will show a decrease in ΔD. Peptides that reveal changes in deuterium uptake are likely to be located in the binding region, at protein interfaces, or part of other conformational changes associated with ligand binding (*26*−*29*).

In the hTRF2−DNA case, the positively charged residues of lysine and arginine are expected to interact with the major and minor grooves of the DNA and the negatively charged phosphate backbone. These types of interactions would be difficult to follow by H/D exchange because the lysine ϵ-amino group hydrogens exchange too rapidly and the amide hydrogens may not be more protected upon ligand binding. Selective modification of certain amino acid residues, in particular the ϵ-amino group of lysine, should be more suitable for probing this type of interaction (*30*−*34*); acetylation seems to be an appropriate method. The most common reagent for acetylation is acetic anhydride; however, there have been numerous examples of other reagents developed to target the reactive primary amine on lysine (*30*, *32*, *35*−*38*). A diminished level of acetylation of lysine side chains of hTRF2 upon binding should provide complementary information regarding the interaction with DNA.

We describe here the application of an improved PLIMSTEX methodology, incorporating the localized deuterium uptake of individual peptic peptides in the protein sequence, and side chain modification (acetylation) to access the DNA binding properties of hTRF2. We are motivated by our interest in not only the protein but also protein−DNA interactions, a topic of importance in biophysics (*39*, *40*).

EXPERIMENTAL PROCEDURES

Materials. Deuterium oxide, potassium chloride, formic acid, acetic anhydride, HEPES [*N*-(2-hydoxyethyl)piperazine-*N*′-2-ethanesulfonic acid], and HEPES sodium salt were purchased from Sigma-Aldrich (St. Louis, MO). The model of telomeric DNA (5′-GTTAGGGTTAGGG-3′) and its complement were purchased from Integrated DNA Technologies (Coralville, IA), analyzed by mass spectrometry for purity, and used without further purification. Immobilized pepsin on agarose was purchased from Pierce (Rockford, IL).

Protein Expression and Purification. The DNA-binding domain of human telomeric repeat binding factor 2 (hTRF2) was overexpressed in *Escherichia coli* [BL21(DE3) from Novagen]. The cells were grown at 37 °C, and the protein expression was induced by the addition of 1 mM isopropyl 1-thio-β-D-galactopyranoside (IPTG) when the OD_{600} reached 0.5−0.6. After additional cell growth at 37 °C for 2.5 h, the cells were harvested and resuspended in buffer A [50 mM potassium phosphate buffer (pH 7.0), 1 mM EDTA, and 100 mM NaCl]. The cells were lysed by sonication on ice and then centrifuged at 39000*g* for 90 min. The protein was purified with AKTA FPLC at 4 °C. The supernatant was applied to a column of HiLoad 26/10 SP Sepharose (GE Healthcare, Piscataway, NJ), equilibrated with buffer A for 4 h, and the protein was eluted with a linear gradient from buffer A to buffer A′ [50 mM potassium phosphate (pH 7.0), 1 mM EDTA, and 400 mM NaCl] in 6.5 h at a flow rate of 1 mL/min. The sample solution was then loaded on a column of HiLoad 26/60 Superdex 75 pg (GE Healthcare) equilibrated with buffer A″ [50 mM potassium phosphate (pH 7.0), 1 mM EDTA, and 1 M NaCl], and sample fractions of DNA-binding domain of hTRF2 were collected. The collected solution was concentrated with a Vivaspin 20 mL concentrator (molecular weight cutoff of 3000, Sartorius Stedim Biotech, Aubagne, France) to 22.5 mg/mL. The concentrated sample was divided into 1.5 mL tubes, lyophilized, and stored in a freezer before use.

Formation of Duplex DNA. Equimolar amounts of the complementary single-stranded oligodeoxynucleotides (ODN) were mixed in a 10 mM HEPES buffer containing 150 mM KCl. The solution temperature was increased to 95 °C and then decreased by 5 °C every 30 min until it reached 25 °C. Duplex formation was monitored by UV spectrophotometry at 260 nm, affording a transition temperature (T_m) of 49 ± 2 °C.

H/D Exchange Protocol. Protein stock solutions were prepared so that they contained 10 mM HEPES (pH 7.4) and 150 mM KCl. Titration experiments started with the equilibration of hTRF2 with varying concentrations of the model ODN for 1 h. To initiate exchange, 0.5 μL of the protein stock was diluted with 20 μL of D_2O containing 10 mM HEPES and 150 mM KCl at 25 °C. At various times, the exchange is quenched with 1.0 M ice-cold HCl to give a final pH of 2.0.

For global deuterium uptake data, the quenched solution was loaded on a C_8 guard column (1 mm × 15 mm, Optimize Technologies, Oregon, City, OR), pre-equilibrated with 100 μL of 0.2% formic acid in water (0 °C), and washed with 300 μL of 0.2% formic acid in water (0 °C), back-exchanging the labile sites of the protein (i.e., those fast exchanging sites, most of which are on side chains). The protein was eluted with an isocratic flow of 40% solvent B at 40 μL/min (Waters CapLC; solvent A, 95% water and 5% acetonitrile containing 0.3% formic acid; solvent B, 5% water and 95% acetonitrile containing 0.3% formic acid). This is slightly modified from the previously reported protocol (*22*, *41*).

For local deuterium uptake data, 5 μL of immobilized pepsin on agarose was added to the quenched solution. The digestion took place for 3 min at 0 °C with a quick vortexing pulse every 15 s. After digestion, the beads were briefly centrifuged (2−3 s) so that they congregated at the bottom of the sample tube, and the digested protein solution was loaded on a C_{18} column (1 mm × 15 mm, PepMap cartridge, LC Packings, Sunnyvale, CA) that was pre-equilibrated with

100 μL of 0.2% formic acid in water (0 °C). The column was washed with 300 μL of 0.2% formic acid in water (0 °C), back-exchanging the labile sites of the peptides and undigested protein. The peptides were separated with a LC gradient (10 to 35% B over 8 min, 35 to 100% B over 3 min, back to 10% B for equilibration). To minimize back-exchange, the incoming/outgoing LC solvent line, injection valve, and sample loop were submerged in ice (0 °C).

High concentrations of the model ODN interfered with protein detection by MS, giving extensive protein signal suppression. Therefore, it was necessary to add an anion exchange guard column (Optimize Technologies, 1 mm × 15 mm) to reduce the ODN concentration effect. The column trapped the ODN while passing the protein, leading to significantly increased protein signals. In this case, the column washing procedure was the same as that described above; however, after elution of protein into the mass spectrometer, the column was washed with 300 μL of aqueous sodium hydroxide (pH 9) to elute the ODN to waste.

Acetylation Protocol. Acetylation with acetic anhydride took place with the same solutions of protein that were used for the H/D exchange experiment, with and without ligand present, as described above. The addition of 0.5 μL of acetic anhydride to the protein in aqueous buffer [10 mM HEPES and 150 mM KCl (pH 7.4)] gave an ∼28000-fold molar excess of reagent per site of acetylation. The solution was allowed to react for various times and quenched at pH 2.0 with 1 M HCl. The solution was digested with immobilized pepsin on agarose, injected onto a C_{18} column, desalted, and eluted into the mass spectrometer, as described above.

LC−ESI/MS Analysis with a Q-TOF Mass Spectrometer. All ESI mass spectra were acquired in positive-ion mode on a Waters (Micromass) (Manchester, U.K.) Q-TOF Ultima spectrometer equipped with a Z-spray ESI source. The capillary voltage was 3.2 kV, with a cone voltage readback of 100 V, and the source and desolvation temperatures were 80 and 180 °C, respectively. The cone and desolvation gas flows were 40 and 400 L/h, respectively. The MS profile used for quadrupole transmission was as follows: from *m*/*z* 500, dwell for 5% of the scan time, ramp to *m*/*z* 1000 for 45% of the scan time, and then dwell at *m*/*z* 1000 for 50% of the scan time.

LC−ESI-MS/MS Analysis of Protein Digest. Peptides produced by pepsin cleavage were identified by accurate mass and product-ion sequencing on a LTQ-FTMS instrument (Thermo, San Jose, CA) and then searched against a database using Mascot (Matrix Science, Oxford, U.K.). After pepsin digestion for 3 min, following the protocol described above, the solution was loaded onto a C_{18} custom-packed column (75 μm inside diameter, 10 cm length). The peptides were separated over 70 min using an Eksigent (Dublin, CA) NanoLC-1D column with an LC gradient from 3 to 97% acetonitrile containing 0.1% formic acid at 260 nL/min. The solution was sprayed directly from the column into the mass spectrometer using a PicoView PV-500 nanospray source (New Objective, Woburn, MA) attached to the LTQ-FTMS instrument. A full mass spectrum was recorded in the FT part of the instrument, operating at a mass resolving power of 100 000 at *m*/*z* 400, and data-dependent product-ion scans of precursors identified by the FTMS were collected by the ion trap. The MS/MS experiments carried out in the LTQ instrument utilized wide-band activation and dynamic exclusion.

Data Analysis. The protein mass spectrum at each H/D exchange time point was deconvoluted using the MaxEnt1 algorithm (MassLynx version 4.0). The deuterium level at each time point was determined by subtracting the average mass of the undeuterated protein from the average mass of the deuterated protein. The rate of back-exchange was measured to be one deuterium lost per minute. The protein deuterium uptake was not corrected for back-exchange because the time from quench to observation in the mass spectrometer is less than 2 min. Ion signals for the deuterated peptides were smoothed twice in MassLynx with a Savitsky−Golay algorithm and imported into Microsoft Excel as an *x*, *y* pair (mass, intensity). The centroid and width of the deuterium distribution for each peptide were analyzed using HX-Express (*42*). The back-exchange occurs at the same rate as in the global experiment; however, no corrections were made for this deuterium loss because only relative (not absolute) deuterium levels need to be compared in all experiments. The methods for fitting the deuterium uptake kinetic data and the PLIMSTEX curve were described previously (*23*). All of the experiments were conducted in triplicate.

RESULTS

Global H/D Exchange Deuterium Uptake Kinetics. A logical starting point for this investigation is the forward H/D exchange reaction kinetics, which we carried out over a 60 min time course. A plot of the deuterium uptake versus time of H/D exchange for the apo and holo forms of hTRF2 shows the protection change due to hydrogen bonding and/or solvent accessibility (Figure 1A). The maximum amount of deuterium incorporation at backbone amides occurred when the apoprotein exchanged for 5 h at 37 °C. The maximum mass shift of 60 Da is in agreement with the number of amide hydrogens available for exchange (62), corrected for the percent D_2O used in the experiments (97%). We fit the data by using a three-group, pseudo-first-order kinetics model to give the distribution of fast-, intermediate-, and slow-exchanging amide hydrogens (*43*). The apo state has approximately 32 fast-exchanging hydrogens with a rate constant of 55 min^{-1}, 25 intermediate-exchanging hydrogens with a rate constant of 0.8 min^{-1}, and two slow-exchanging hydrogens with a rate constant of 0.1 min^{-1}. The holo state has fewer fast-exchanging hydrogens (∼28) with a rate constant of 14 min^{-1}, 10 intermediate-exchanging hydrogens with a rate constant of 0.3 min^{-1}, and many more slow-exchanging hydrogens (∼20) with a rate constant of 0.03 min^{-1}.

After exchange for 2 min, the apoprotein exhibited a mass shift of >50 Da, suggesting the DNA-binding domain of hTRF2 has many fast-exchanging amide sites without any ligand present. The apoprotein approached the maximum Δ*D* after H/D exchange for 10 min. Incorporation of the ODN at a 10:1 ratio with respect to the concentration of the protein (1 μM) produces the holo form of the complex. The 10:1 complex has a reduced level of deuterium uptake at all times, although the maximum level of uptake is similar at 60 min. This difference in deuterium uptake indicates that the individual amide H/D exchange rates decrease upon com-

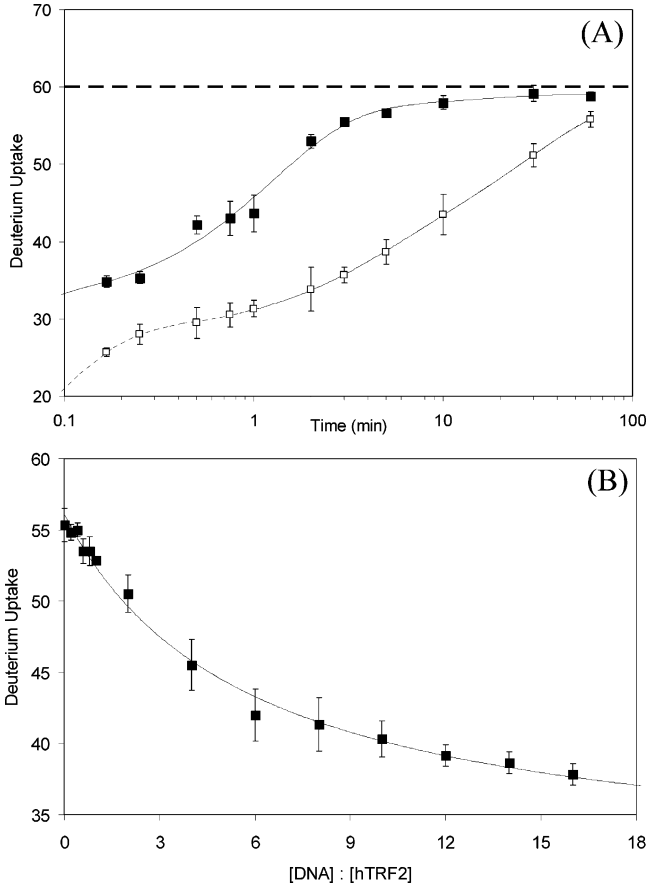

FIGURE 1: (A) Global deuterium uptake kinetics over a 60 min time course for apo (■) and holo (□) hTRF2 (1 μM). The maximum deuterium uptake (− − −) was achieved at 37 °C after 5 h. (B) PLIMSTEX titration curve obtained by monitoring the deuterium uptake of hTRF2 (100 nM) with increasing amounts of the model ODN. The H−D exchange time of 3 min was held constant during the titration. A K_D of 580 ± 140 nM, a ΔD of 25.1 ± 1.5 Da, and a D_0 of 56.1 ± 0.4 Da were output from the PLIMSTEX modeling.

plexation with the ligand. The maximum deuterium difference (ΔD) occurs at 3 min of H/D exchange.

PLIMSTEX Titration. A titration of hTRF2 with increasing amounts of the model telomeric ODN at a fixed H/D exchange time (Figure 1B) yields information regarding the dissociation constant. The extent of deuterium uptake decreases with addition of increasing amounts of ligand, and the final state reaches a similar level of uptake as seen in the H/D exchange kinetics for the 10:1 complex. The deuterium uptake data were fit with a nonlinear least-squares 1:1 ligand binding model, as previously described (*23*).

The concentration of hTRF2 for the titration experiments was 100 nM, a concentration that is approximately equal to the K_D determined previously (*12*). We chose that concentration to ensure that when the stoichiometric amount of ligand was added, there was a measureable amount of free ligand in solution. The output of the nonlinear fitting produces a K_D of 580 ± 140 nM, which agrees with the previously reported value within a factor of 3. The parameters D_0 (56.1 ± 0.4 Da), which represents the deuterium uptake in the apo state at the specified time, and ΔD (25 ± 2 Da) also fit the experimentally observed data. When we used the affinity constant determined by PLIMSTEX to calculate the fractional bound species, we found a value of 78%, in good agreement

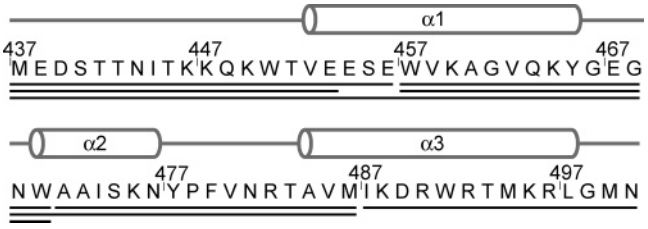

FIGURE 2: hTRF2 DNA-binding domain sequence that contains a portion of the unstructured linker (residues 437−451) and the conserved three-helix bundle. Peptides generated by pepsin cleavage are underlined. Seven peptides covering 100% of the sequence were identified and analyzed by mass spectrometry. The two peptides starting at residue 457 continue to residues 470 and 486. The peptide starting at 437 continues to residue 470.

with the experimental value of 77% holo formation when the ratio of DNA to hTRF2 is 16:1.

H/D Exchange Deuterium Uptake Kinetics for Regions of the Protein. An important goal in the development of PLIMSTEX is to explore the deuterium exchange of component peptides throughout a protein of interest. Our previous studies of calmodulin, intestinal fatty acid binding protein, and insulin focused on the global H/D exchange view of protein function and dynamics (*21*, *41*, *44*). Expanding the resolution to the peptide level will provide site-specific information regarding how the protein changes conformation upon interacting with a ligand of interest.

Digestion of the deuterated protein with pepsin affords 22 unique peptides. Most peptides are variants of a set of four that differ by the addition or subtraction of one or two amino acid residues from the N- or C-terminal end. Pepsin tends to cleave near hydrophobic residues, which are scarce in the DNA-binding domain of hTRF2. As a result, we did not observe many overlapping regions. The peptides were sequenced by obtaining both their product-ion spectra and accurate masses in an LC−MS/MS experiment conducted on an ion trap/Fourier transform mass spectrometer. Unfortunately, we were unable to observe all of the peptides found with the nanospray ion-trap/FT system on the Q-TOF instrument, most likely because of the difference in sensitivity and the source configurations of the two instruments. The list of observed peptides on the Q-TOF instrument (Figure 2) was generated from those that were detected with sufficient signal-to-noise ratios to afford reliable deuterium uptake data as well as complete coverage of the protein. Following the kinetics of deuterium incorporation for the individual peptides, we were able to determine those regions of hTRF2 that are protected and those that are unaffected by the binding to the ODN (Figure 3).

Peptides 437−453 and 437−456 are located in the flexible linker region of full-length hTRF2. Both peptides, with no ligand present, are highly deuterated (~81 and 84%, respectively), reaching this exchange after a short deuteration period of 1 min. There is no change in the deuterium uptake of peptide 437−453 when there is ligand present, indicating that the peptide has a similar hydrogen bonding network in both apo and holo states. Peptide 437−456, upon binding the ODN, shows a slight decrease in the extent of deuterium uptake (~2−3 Da) between 1 and 3 min of H/D exchange. Residues 454−456, represented by the difference in the two peptide sequences, must reveal some secondary structure in this region. Two peptides that are affected significantly by

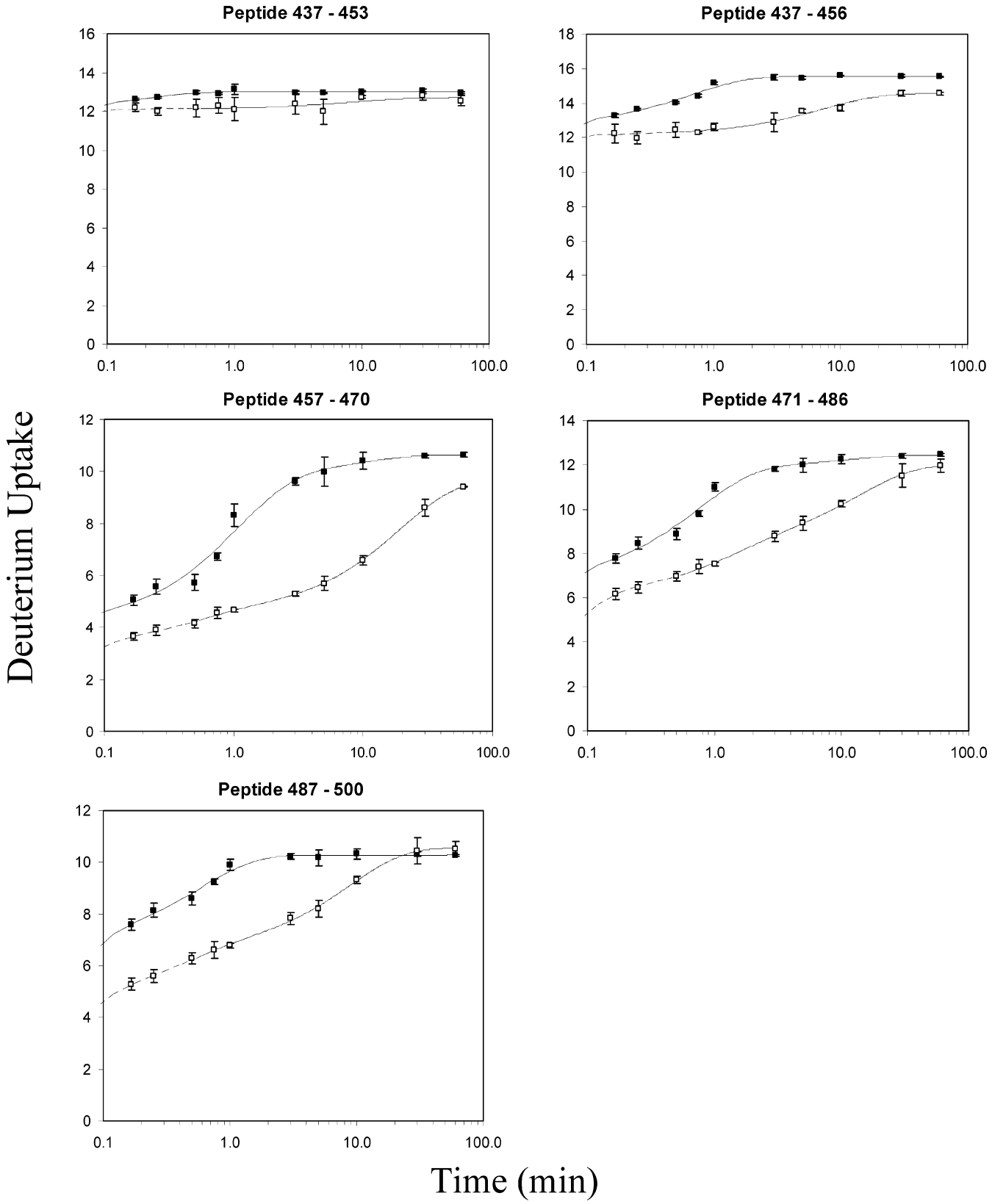

FIGURE 3: Kinetics of incorporation of deuterium into several peptides of hTRF2 (12 μM) in the apo (—) and ODN-bound form (- - -). The holo state has a 2:1 ratio of DNA to hTRF2.

binding, arbitrarily defined as a ΔD_{max} of >25% of the exchangeable residues, are 457−470 and 471−486. After 3 min of H/D exchange, the ΔD for peptide 457−470 is at its maximum, representing more than 35% of the exchangeable amide sites taking up D. The ΔD of peptide 471−486 at 3 min of H/D exchange exchanged more than 25% of the amide sites. These extents of amide exchange are influenced by the binding of DNA, indicating that these regions of the protein are part of the interaction network. The helix responsible for the major grove interaction is part of peptide 487−500. The extent of amide exchange decreases compared to that of the apo state, and the ΔD_{max} occurs at

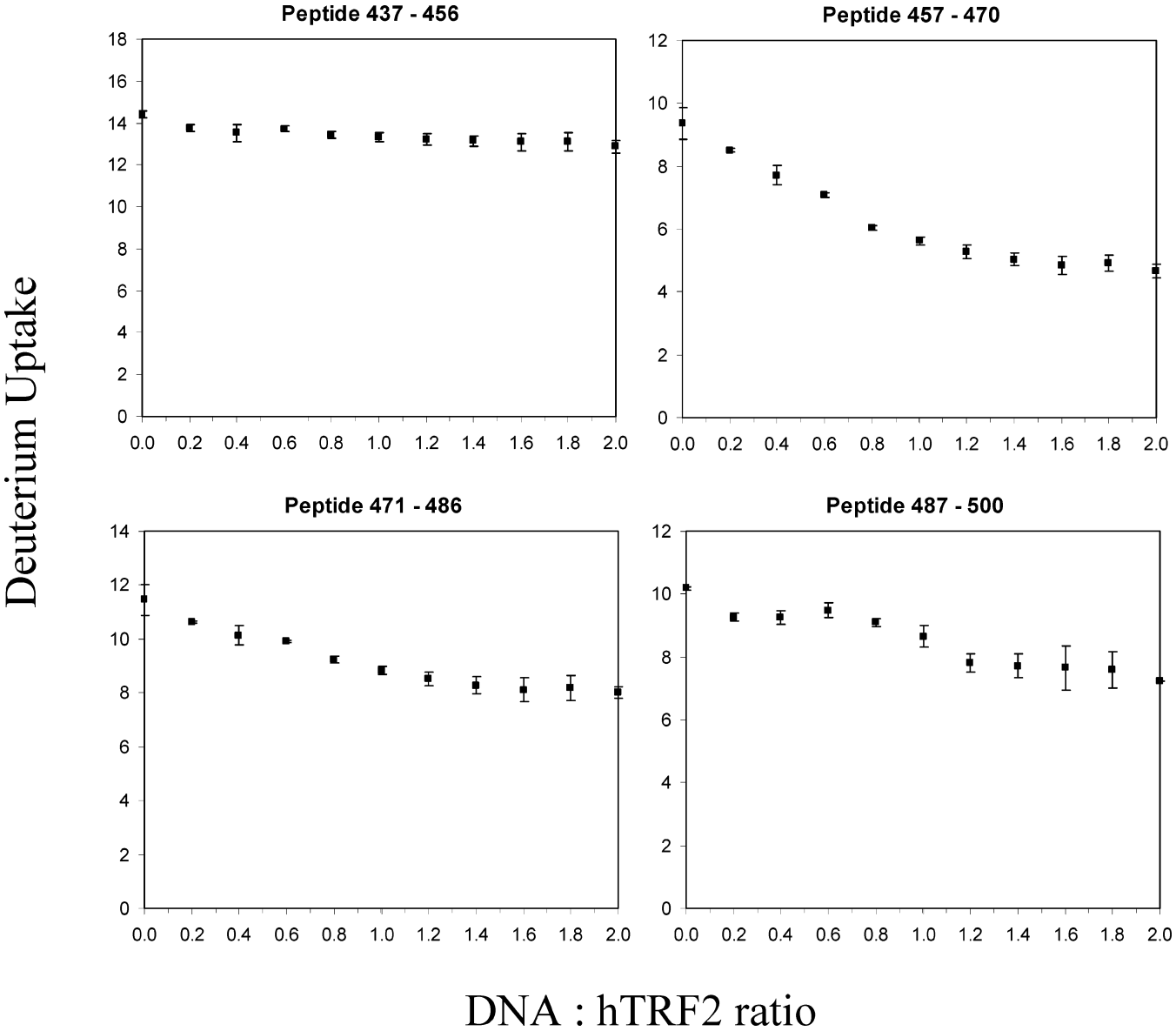

FIGURE 4: High-resolution titration of hTRF2 (12 μM) with increasing amounts of ODN present. The H/D exchange time of 3 min is held constant during the titration.

1 min of amide exchange. The holo deuterium uptake curve approaches the apo curve in a shorter time than for the other peptides. At first thought, one might expect that this portion of hTRF2 would undergo the largest change in deuterium uptake when the telomeric ODN binds, given that this part of the DNA-binding domain interacts in the major groove.

PLIMSTEX Titrations for Various Regions of the Protein. To probe the equilibrium binding of the telomeric ODN at various locations of hTRF2, we performed a titration and measured the extent of H/D exchange for various peptide regions of the protein. This experiment reveals how the deuterium uptake changes with increasing amounts of ligand at the peptide level of resolution. The experiment was conducted at a high protein concentration (12 μM), which is 2 orders of magnitude above the reported K_D, to ensure stoichiometric binding of the model telomeric DNA. Carrying out an H/D exchange experiment of this type produces a "sharp break" titration curve when the intact protein is titrated with ligand and reveals the binding stoichiometry (*21*, *22*). The largest changes in deuterium uptake take place at a ligand concentration ratio of less than 1:1, consistent with the stoichiometry as one hTRF2 binding domain for one telomeric ODN sequence motif (e.g., see Figure 4, peptide 457−470).

All peptides except 437−456 show obvious decreases in the extent of deuterium uptake as seen when substoichiometric (i.e., 0.2 equiv) of the model telomeric ODN is present. Peptides 457−470 and 471−486 show a regular decrease in the level of deuterium uptake as increasing amounts of the ligand are added, whereas peptide 487−500 shows a more irregular pattern of deuterium uptake with an increase in ligand concentration. For the latter, the deuterium uptake remains relatively constant until the added ligand concentration reaches the stoichiometric 1:1 binding point and then decreases to another plateau of deuterium uptake. One might expect that the sum of the amplitudes of these curves would be equal to the ΔD found in the titration of the intact protein. One means of assessing this is to compare the extent of exchange in the apo state of the four peptides (437−456, 457−470, 471−486, and 487−500) that represent 100% coverage to the extent of exchange exhibited by the

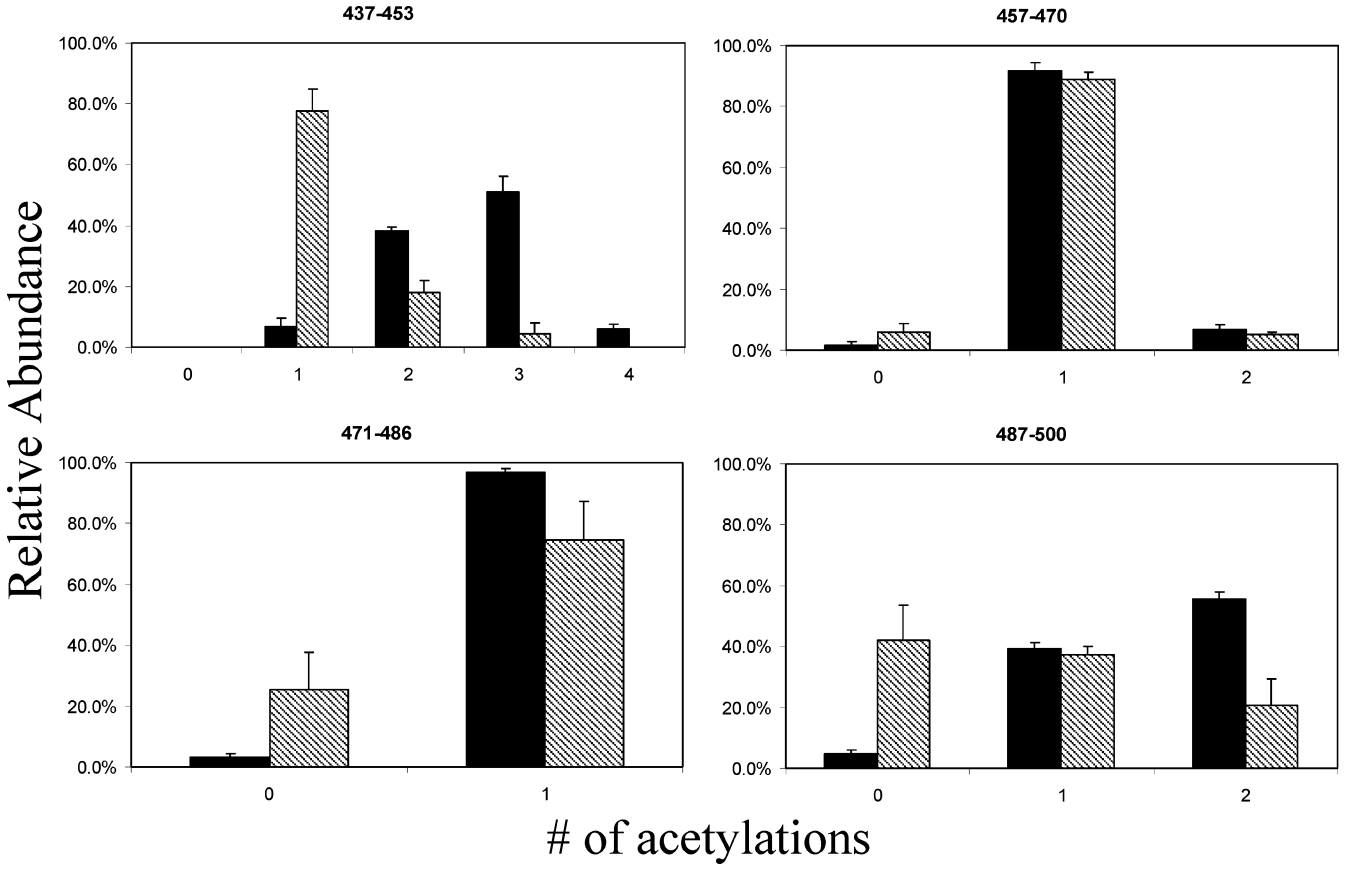

FIGURE 5: Summarized acetylation data for four peptides of apo (black) and holo (cross-hatched) hTRF2. The data are normalized intensities of the monoisotopic peak from three experimental trials of the apo and ODN-bound state. The distribution of acetylation changes in peptides 437−453 and 487−500, while it remains constant in peptides 457−470 and 471−486.

apoprotein. The sum for the peptides is 46, whereas 55 amides of the apoprotein undergo exchange (compare Figures 1B and 4). Although the rates of back-exchange are the same in the global and high-resolution PLIMSTEX experiments, the extent of back-exchange of the apoprotein is considerably smaller than those of the constituent peptides. This occurs because the protein mass is measured within 2 min of quenching the exchange, whereas the peptides are produced in a digestion and introduced to ESI via HPLC. The latter two steps consume time and allow the peptides to undergo a greater extent of back-exchange. Thus, although a comparison of exchange of the peptide and protein is problematic, the amplitudes in both the kinetics and titration experiments of the individual peptides can be summed and compared because the conditions of the analysis are constant from point to point.

It may be possible to conduct the high-resolution titrations at the same protein concentration as that used in the global titration. We chose, however, to conduct the titration at a higher protein concentration to compress the deuterium uptake over a smaller ligand-to-protein concentration range, thereby providing both the stoichiometry of binding and a determination of those regions of the protein that interact with the ligand. Achieving affinity constants for localized regions of the protein requires that the high-resolution titrations be done at a lower protein concentration and over a larger ligand-to-protein concentration range.

Acetylation of the Binding Sites. We selected another method to probe the specific binding sites between hTRF2 and the model ODN. Given that lysine and arginine residues play a crucial role in the dynamics of binding to telomeric DNA, a selective modification of Lys and/or Arg side chains should be an appropriate approach to probing protein interactions in protein−DNA complexes. Although one could choose to modify arginine residues with dicarbonyl compounds that condense with the guanidinium group on the side chain (*30*, *34*, *45*), the most common form of selective modification is acetylation of the reactive primary amines of lysine. Numerous reagents were developed to target solvent accessible lysines (*30*, *32*, *35*−*38*). We chose to use acetic anhydride because it is readily available and easy to use, even though we had to employ higher concentrations to achieve similar acetylation profiles that are expected with other reagents. One reason for the need for higher concentrations is the hydrolysis half-life of acetic anhydride in aqueous solutions is 4−5 min (*46*).

The protein was digested with pepsin after an acetylation reaction time of 1 min, affording the same set of peptides that are seen in the H/D exchange experiments. The decrease in the acetylation patterns of peptides 437−453 and 487−500 is noticeable even at the short acetylation time period (Figure 5). Peptides 457−470 and 471−486 do not show any change in their acetylation pattern in the presence or absence of the ODN. Peptides 457−470 and 471−486 have two possible sites and one possible site of acetylation, respectively. The patterns for both of these peptides show relatively little change in their acetylation distributions. By way of contrast, the H/D exchange showed that these two peptides have the largest change in the amide hydrogen bonding network in hTRF2.

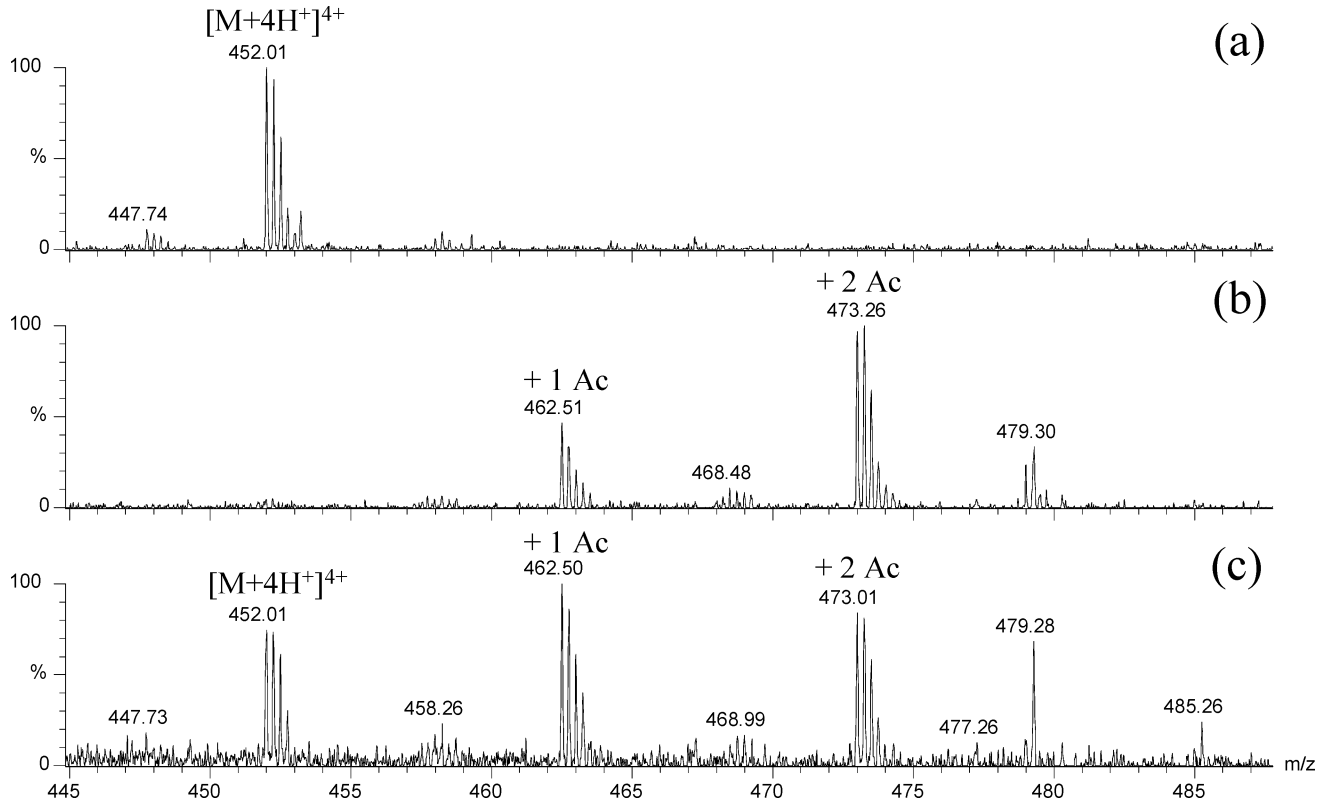

FIGURE 6: ESI mass spectra of peptide 487−500 [M + 4H$^+$]$^{4+}$ with (a) no acetylation, (b) the apoprotein acetylated, and (c) the holoprotein acetylated. The acetylation reaction was allowed to proceed for 1 min. The amounts of non- and monoacetylation increase in the holo state of the protein.

The portion of hTRF2 that binds in the major groove of the model telomeric DNA is peptide 487−500. There are two possible acetylation sites on this peptide: Lys 488 and 495. For the apo state, the distribution of acetylation centers at 1.5, and the most probable amount of acetylation is two. In the presence of the model telomeric ODN, the distribution of acetylation decreases to slightly less than one modification (Figure 6). There is a significant increase in the amount of unmodified peptide with a concomitant decrease in the doubly acetylated form. This decrease in acetylation indicates that peptide 487−500 is shielded from solvent while interacting with the telomeric ODN. There are four possible sites of acetylation on peptide 437−453, including Lys 446, 447, and 449 and the N-terminus of the DNA-binding domain of hTRF2. For the apo state, a distribution of one to four acetylations occurs, centered between two and three modifications. In the holo state, the acetylation distribution shifts to a lower extent, with no visible signal for four modifications. Interestingly, the H/D exchange data for this particular peptide show no change between the apo and holo states.

DISCUSSION

The advantages of PLIMSTEX are that it is a measure of solution (not gas-phase) equilibrium, can be used in any buffer, and does not require any tethering or additional labeling of the protein or ligand. A previous experiment conducted by using surface plasmon resonance (SPR) yields a dissociation constant (K_D) of 180 nM (*12*), which is a factor of 3 different from the value determined by PLIMSTEX. SPR is an accepted means of measuring dissociation constants; its major drawback is that either the macromolecule of interest or the ligand must be tethered to a surface (*47*). For the binding of hTRF2, the measurement was made by tethering the model DNA to the surface and injecting the DNA-binding domain of hTRF2 over the surface (*12*). This tethering may not provide an accurate representation of a solution affinity. PLIMSTEX, on the other hand, requires no tethering and affords the solution-phase affinity. It requires no special labeling (e.g., fluorescent tagging) of either species or other physical changes to the system.

The high-resolution PLIMSTEX technique, a modified version of global PLIMSTEX, incorporates pepsin digestion and LC−MS measurements to localize deuterium uptake at the peptide level. This increased spatial resolution of deuterium uptake provides information about the peptide binding dynamics with varying amounts of ligand present. The data can be compared to structural information revealed by NMR and X-ray crystallography techniques to validate the amide exchange methodology. Most of the large changes in deuterium uptake of individual peptides are in regions that do not contain side chain contacts to the ligand but are in those that contain contacts through amide hydrogens or that undergo an overall tightening of the amide hydrogen bonding network.

There was a noticeable difference in the deuterium uptake of peptides 437−453 and 437−456, even though only three amino acids (454−456) differentiate the two peptic peptides. According to the NMR and X-ray crystallography structures, these residues are part of a region that has α-helical character, which explains the difference in deuterium uptake between the two peptides. Amide hydrogens involved in an α-helix will exchange more slowly than those that are unstructured and not involved in hydrogen bonding. Peptides 437−453 and 437−456 contain Lys 447, which contacts T9 in the

minor grove of the model telomeric ODN. This binding does not affect the deuterium uptake of the two peptides, which is revealed in the high-resolution PLIMSTEX titration. The deuterium uptake remains constant upon addition of the ODN because the hydrogens on the lysine side chain exchange too rapidly to be observed in the mass spectrometric H/D exchange experiment.

The deuterium uptake of peptides 457−470 and 471−486 reveals sites of protection present when the ODN is bound. The holo structure, as determined by NMR, reveals an amide contact of Ala 471 to the phosphate group of T3. The amide nitrogens of Trp 470 and Asn 469 are also in the proximity of the phosphate backbone. The involvement of these amide hydrogens with the backbone will slow the exchange rate with deuterium. The high-resolution PLIMSTEX titration of these two peptides reveals their deuterium uptake change with an increase in the amount of ligand. At high concentrations of protein, very little free ligand is present in solution. This allows the measurement of an absolute deuterium change upon binding the ODN. Peptide 457−470 behaves like the whole protein in that the major deuterium uptake change takes place from no ligand to the stoichiometric amount of 1:1. The ΔD at 3 min of H/D exchange is ~5 with more than 90% of the change taking place before the ligand concentration reaches the stoichiometric point. The deuterium uptake remains relatively constant after 1 equiv of the ODN is added. The ΔD of peptide 471−486 at 3 min of H/D exchange is ~3.5. Similarly, upon addition of the ligand, more than 90% of the deuterium uptake change takes place before the 1:1 binding point.

The helix responsible for the major grove interaction is part of peptide 487−500. At first thought, one might expect that this portion of hTRF2 would undergo the largest change in deuterium uptake when the telomeric ODN binds. When comparing the apo and holo NMR structures, however, the actual amide hydrogen network of the α-helix remains relatively constant in both states. Since there is no change in the conformation of the helix, the decrease in amide exchange rates for this peptide is an example of the hydrogen bonding network undergoing an overall tightening upon binding the ODN. The high-resolution PLIMSTEX titration reveals a shift of one deuterium upon binding 0.2 equiv of ODN, which may indicate a stabilization of the helix upon lysine and/or arginine interacting with the ODN binding site. This deuterium shift does not change upon binding additional ligand up to the 1:1 stoichiometric point. Upon addition of 1 equiv of the ODN, a second shift in deuterium uptake occurs, a decrease of an additional deuterium. After this change, the deuterium uptake remains relatively constant; however, there is a general downward trend at 2 equiv.

To judge the effectiveness of acetylation, we obtained the solvent accessibilities of the hTRF2 lysine residues by using GETAREA (*48*). Using the 25 apo NMR structures (PDB entry 1VF9) and the 20 holo NMR structures (PDB entry 1VFC), we averaged the solvent accessibilities (see Table 1 for a comparison). Lys 447 and 488 show a dramatic decrease in solvent accessibility in the holo form; Lys 449 has a slight decrease, and the solvent accessibilities of all other lysines remain relatively constant. Lys 447 interacts with T9 in the minor groove, whereas Lys 488 interacts with G5 and G6 in the major groove.

Table 1: Solvent Accessibilities of All Lysine Side Chains in hTRF2[a]

Lys	apo (Å^2)	holo (Å^2)
446	146.9 ± 18.8	118.4 ± 37.8
447	134.1 ± 22.6	26.6 ± 5.4
449	139.4 ± 20.3	108.6 ± 27.7
459	118.7 ± 12.3	106.9 ± 11.0
464	122.6 ± 7.6	131.5 ± 14.5
475	144.4 ± 9.5	149.9 ± 3.3
488	96.6 ± 10.2	10.5 ± 3.9
495	110.6 ± 13.6	94.3 ± 9.5
average	71.8 ± 9.8	61.0 ± 8.6

[a] A total of 25 apo structures and 20 holo structures were used to calculate the solvent accessibilities. A comparison of lysines to the average of all residue side chains shows the relative solvent exposure in each state. Lys 447 and 488, as well as Lys 449, undergo a decrease in solvent accessibility in the ODN-bound state. Calculated using GETAREA.

Peptides that contain Lys 447, 449, and 488 all exhibited a decrease in their acetylation distributions when the protein binds the ligand, in agreement with the solvent accessibility data. Although peptides 437−453 and 437−456, which contain Lys 447 and 449, have consistent shifts in acetylation patterns, they show no real change in conformation from the amide exchange experiments. Peptides 457−470 and 471−486, however, show no distinct change in acetylation, and this agrees well with the solvent accessibility data. Although the side chains are not involved in binding the telomeric ODN, their amide backbones do contact the phosphate groups, causing a tightening of the helical structure that is revealed by a change in the extent of H/D exchange.

The results of the H/D exchange and acetylation experiments afford complementary information regarding the binding of hTRF2 to the model telomeric DNA. The hTRF2−telomeric DNA model affords the opportunity to compare the effects on H-bonding of amide hydrogens when a protein binds an ODN ligand, both at the site of interaction and at sites remote from the binding. The extent of the acetylation reaction, on the other hand, reveals the decrease in solvent accessibility of those lysines involved in the binding of the telomeric ODN. Although other chemical probes can target different side chains (e.g., OH radicals and various cross-linking agents), acetylation with acetic anhydride is a simple and effective approach to monitoring solvent accessibility of lysine in DNA-binding proteins. If these observations are general, we expect that regions of a protein that have specific side chain contacts to phosphates or DNA bases will show relatively little difference in the extent of H/D exchange but significant decreases in acetylation as DNA binding occurs. In the case of hTRF2, the N-terminal linker and the third helix undergo relatively little change in the extent of H/D exchange but show decreases in the solvent accessibility of lysines upon binding the ODN ligand. The technique may be applicable to other protein systems where information regarding ligand-induced cooperativity is sought. The combined approach allows one to observe areas of a protein that change their deuterium uptake with relatively little ligand present and to follow those changes (via a titration) as the extent of binding is increased. Although we developed this approach to probe the hTRF2 DNA-binding domain, we wish to expand the method to full-length proteins that are difficult to study by other structure-based methods.

We also acknowledge the prospect of a high-resolution PLIMSTEX approach for giving affinity for regions of a protein. This is the subject of future research.

ACKNOWLEDGMENT

We thank Dr. Henry Rohrs for assistance with the LTQ-FTMS studies and the database searching.

REFERENCES

1. Bilaud, T., Brun, C., Ancelin, K., Koering, C. E., Laroche, T., and Gilson, E. (1997) Telomeric localization of TRF2, a novel human telobox protein, *Nat. Genet. 17*, 236−239.
2. Broccoli, D., Smogorzewska, A., Chong, L., and de Lange, T. (1997) Human telomeres contain two distinct Myb-related proteins, TRF1 and TRF2, *Nat. Genet. 17*, 231−235.
3. Chong, L., Steensel, B. v., Broccoli, D., Erdjument-Bromage, H., Hanish, J., Tempst, P., and de Lange, T. (1995) A human telomeric protein, *Science 270*, 1663−1667.
4. Steensel, B. v., and de Lange, T. (1997) Control of telomere length by the human telomeric protein TRF1, *Nature 385*, 740−743.
5. Smogorzewska, A., and de Lange, T. (2004) Regulation of telomerase by telomeric proteins, *Annu. Rev. Biochem. 73*, 177−208.
6. de Lange, T. (2002) Protection of mammalian telomeres, *Oncogene 21*, 532−540.
7. de Lange, T. (2004) T-Loops and the origin of telomeres, *Nat. Rev. Mol. Cell Biol. 5*, 323−329.
8. Munoz, P., Blanco, R., and Blasco, M. A. (2006) Role of the TRF2 telomeric protein in cancer and ageing, *Cell Cycle 5*, 718−721.
9. Fairall, L., Chapman, L., Moss, H., de Lange, T., and Rhodes, D. (2001) Structure of the TRFH dimerization domain of the human telomeric proteins TRF1 and TRF2, *Mol. Cell 8*, 351−361.
10. Bilbille, Y., Paquet, F., Meudal, H., Giraud-Panis, M.-J., and Lancelot, G. (2006) NMR studies of telomeric nucleoprotein complexes involving the Myb-like domain of the human telomeric protein TRF2, *C. R. Chim. 9*, 452−458.
11. Court, R., Chapman, L., Fairall, L., and Rhodes, D. (2005) How the human telomeric proteins TRF1 and TRF2 recognize telomeric DNA: A view from high-resolution crystal structures, *EMBO Rep. 6*, 39−45.
12. Hanaoka, S., Nagadoi, A., and Nishimura, Y. (2005) Comparison between TRF2 and TRF1 of their telomeric DNA-bound structures and DNA-binding activities, *Protein Sci. 14*, 119−130.
13. Nishikawa, T., Nagadoi, A., Yoshimura, S., Aimoto, S., and Nishimura, Y. (1998) Solution structure of the DNA-binding domain of human telomeric protein, hTRF1, *Structure 6*, 1057−1065.
14. Nishikawa, T., Okamura, H., Nagadoi, A., König, P., Rhodes, D., and Nishimura, Y. (2001) Solution structure of a telomeric DNA complex of human TRF1, *Structure 9*, 1237−1251.
15. Hanaoka, S., Nagadoi, A., and Nishimura, Y. (2006) Comparison of DNA-binding activities between hTRF2 and hTRF1 with hTRF2 mutants, *Mod. Magn. Reson. 1*, 739−747.
16. Engen, J. R., and Smith, D. L. (2001) Investigating protein structure and dynamics by hyrdogen exchange MS, *Anal. Chem. 73*, 256A−265A.
17. Maier, C. S., and Deinzer, M. L. (2005) Protein conformations, interactions, and H/D exchange, *Methods Enzymol. 402*, 312−360.
18. Weis, D. D., Kaveti, S., Wu, Y., and Engen, J. R. (2007) Probing protein interactions using hydrogen-deuterium exchange mass spectrometry, in *Mass Spectrometry of Protein Interactions* (Downard, K., Ed.) John Wiley & Sons, New York.
19. Wales, T. E., and Engen, J. R. (2006) Hydrogen exchange mass spectrometry for the analysis of protein dynamics, *Mass Spectrom. Rev. 25*, 158−170.
20. Englander, S. W. (2006) Hydrogen exchange mass spectrometry: A historical perspective, *J. Am. Soc. Mass Spectrom. 17*, 1481−1489.
21. Zhu, M. M., Chitta, R., and Gross, M. L. (2005) PLIMSTEX: A novel mass spectrometric method for the quantification of protein-ligand interactions in solution, *Int. J. Mass Spectrom. 240*, 213−220.
22. Zhu, M. M., Rempel, D. L., Du, Z., and Gross, M. L. (2003) Quantification of protein-ligand interactions by mass spectrometry, titration, and H/D exchange: PLIMSTEX, *J. Am. Chem. Soc. 125*, 5252−5253.
23. Zhu, M. M., Rempel, D. L., and Gross, M. L. (2004) Modeling data from titration, amide H/D exchange, and mass spectrometry to obtain protein-ligand binding constants, *J. Am. Soc. Mass Spectrom. 15*, 388−397.
24. Zhang, Z., and Smith, D. L. (1993) Determination of amide hydrogen exchange by mass spectrometry: A new tool for protein structure elucidation, *Protein Sci. 2*, 522−531.
25. Garcia, R. A., Pantazatos, D., and Villarreal, F. J. (2004) Hydrogen/deuterium exchange mass spectrometry for investigating protein-ligand interactions, *Assay Drug Dev. Technol. 2*, 81−91.
26. Redeker, V., Halgand, F., Caer, J.-P. L., Bousset, L., Laprévote, O., and Melki, R. (2007) Hydrogen/deuterium exchange mass spectrometric analysis of conformational changes accompanying the assembly of the yeast prion Ure2p into protein fibrils, *J. Mol. Biol. 369*, 1113−1125.
27. Man, P., Montagner, C., Vernier, G., Dublet, B., Chenal, A., Forest, E., and Forge, V. (2007) Defining the interacting regions between apomyoglobin and lipid membrane by hydrogen/deuterium exchange coupled to mass spectrometry, *J. Mol. Biol. 368*, 464−472.
28. Shi, J., Koeppe, J. R., Komives, E. A., and Taylor, P. (2006) Ligand-induced conformational changes in the acetylcholine-binding protein analyzed by hydrogen-deuterium exchange mass spectrometry, *J. Biol. Chem. 281*, 12170−12177.
29. Hochrein, J. M., Lerner, E. C., Schiavone, A. P., Smithgall, T. E., and Engen, J. R. (2006) An examination of dynamics crosstalk between SH2 and SH3 domains by hydrogen/deuterium exchange and mass spectrometry, *Protein Sci. 15*, 65−73.
30. Glazer, A. N. (1970) Specific chemical modification of proteins, *Annu. Rev. Biochem. 39*, 101−130.
31. Edavettal, S. C., Carrick, K., Shah, R. R., Pedersen, L. C., Tropsha, A., Pope, R. M., and Liu, J. (2004) A conformational change in heparan sulfate 3-*O*-sulfotransferase-1 is induced by binding to heparan sulfate, *Biochemistry 43*, 4680−4688.
32. Scholten, A., Visser, N. F. C., Heuvel, R. H. H. v. d., and Heck, A. J. R. (2006) Analysis of protein-protein interaction surfaces using a combination of efficient lysine acetylation and nanoLC-MALDI-MS/MS applied to the E9:Im9 bacteriotoxin-immunity protein complex, *J. Am. Soc. Mass Spectrom. 17*, 983−994.
33. Steiner, R. F., Albaugh, S., Fenselau, C., Murphy, C., and Vestline, M. (1991) A mass spectrometry method for mapping the interface topography of interacting proteins, illustrated by the melittin-calmodulin system, *Anal. Biochem. 196*, 120−125.
34. Suckau, D., Mak, M., and Przybylski, M. (1992) Protein surface topology-probing by selective chemical modification and mass spectrometric peptide mapping, *Proc. Natl. Acad. Sci. U.S.A. 89*, 5630−5634.
35. Janecki, D. J., Beardsley, R. L., and Reilly, J. P. (2005) Probing protein tertiary structure with amidination, *Anal. Chem. 77*, 7274−7281.
36. Kvaratskhelia, M., Miller, J. T., Budihas, S. R., Pannell, L. K., and Grice, S. F. J. L. (2002) Identification of specific HIV-1 reverse transcriptase contacts to the viral RNA:tRNA complex by mass spectrometry and a primary amine selective reagent, *Proc. Natl. Acad. Sci. U.S.A. 99*, 15988−15993.
37. Shell, S. M., Hess, S., Kvaratskhelia, M., and Zou, Y. (2005) Mass spectrometric identification of lysines involved in the interaction of human replication protein A with single-stranded DNA, *Biochemistry 44*, 971−978.
38. Wang, X., Kim, S.-H., Ablonczy, Z., Crouch, R. K., and Knapp, D. R. (2004) Probing rhodopsin-transducin interactions by surface modification and mass spectrometry, *Biochemistry 43*, 11153−11162.
39. Ma, L., and Fitzgerald, M. C. (2003) A new H/D exchange- and mass spectrometry-based method for thermodynamic analysis of protein-DNA interactions, *Chem. Biol. 10*, 1205−1213.
40. Majka, J., and Speck, C. (2007) Analysis of protein-DNA interactions using surface plasmon resonance, in *Analytics of protein-DNA interactions* (Seitz, H., Ed.) pp 13−36, Springer, Berlin.
41. Zhu, M. M., Rempel, D. L., Zhao, J., Giblin, D. E., and Gross, M. L. (2003) Probing Ca^{2+}-induced conformational changes in porcine calmodulin by H/D exchange and ESI-MS: Effect of cations and ionic strength, *Biochemistry 42*, 15388−15397.

42. Weis, D. D., Engen, J. R., and Kass, I. J. (2006) Semi-automated data processing of hydrogen exchange mass spectra using *HX-Express*, *J. Am. Soc. Mass Spectrom. 17*, 1700−1703.
43. Zhang, Z., Post, C. B., and Smith, D. L. (1996) Amide hydrogen exchange determined by mass spectrometry: Application to rabbit muscle aldolase, *Biochemistry 35*, 779−791.
44. Chitta, R. K., Rempel, D. L., Grayson, M. A., Remsen, E. E., and Gross, M. L. (2006) Application of SIMSTEX to oligomerization of insulin analogs and mutants, *J. Am. Soc. Mass Spectrom. 17*, 1526−1534.
45. Hager-Braun, C., and Tomer, K. B. (2002) Characterization of the tertiary structure of soluble CD4 bound to glycosylated full-length HIVgp120 by chemical modification of arginine residues and mass spectrometric analysis, *Biochemistry 41*, 1759−1766.
46. Seoud, O. A. E., Bazito, R. C., and Sumodjo, P. T. (1997) Kinetic solvent isotope effect: A simple, multipurpose physical chemistry experiment, *J. Chem. Educ. 74*, 562−565.
47. McWhirter, A., and Loefaas, S. (2007) Functional analysis of protein interactions using surface plasmon resonance-based microarrays, *Drug Discovery Ser. 8*, 181−198.
48. Fraczkiewicz, R., and Braun, W. (1998) Exact and efficient analytical calculation of the accessible surface areas and their gradients for macromolecules, *J. Comput. Chem. 19*, 319−333.

BI702037P